ELSEVIER

Journal of Organometallic Chemistry 632 (2001) 133–144

Journal of Organometallic Chemistry

www.elsevier.com/locate/jorganchem

Second harmonic generation of η^5-monocyclopentadienyl ruthenium *p*-benzonitrile derivatives by Kurtz powder technique. Crystal and molecular structure determinations of $[Ru(\eta^5\text{-}C_5H_5)((+)\text{-DIOP})(p\text{-}NCC_6H_4NO_2)][X]$, $X = PF_6^-$, $CF_3SO_3^-$ and $[Ru(\eta^5\text{-}C_5H_5)((+)\text{-DIOP})(NCCH_3)][PF_6]$

M. Helena Garcia [a,b,*], João C. Rodrigues [a,c], A. Romão Dias [a], M. Fátima M. Piedade [a,b], M. Teresa Duarte [a], M. Paula Robalo [a,d], Nelson Lopes [e]

[a] *Centro de Química Estrutural, Instituto Superior Técnico, Av. Rovisco Pais, 1049-001 Lisbon, Portugal*
[b] *Faculdade de Ciências da Universidade de Lisboa, Ed. C8, Campo Grande, 1749-016 Lisbon, Portugal*
[c] *Departamento de Química, Universidade da Madeira, Campus Universitário da Penteada, 9000-390, Funchal, Portugal*
[d] *Departamento de Química, Universidade de Évora, Colégio Luís António Verney, Rua Romão Ramalho n° 59, 7000-671 Evora, Portugal*
[e] *GoLP/Centro de Física de Plasmas, Instituto Superior Técnico, 1049-001 Lisbon, Portugal*

Received 26 February 2001; accepted 22 April 2001

On the occasion of the 60th birthday of Professor Alberto Romão Dias

Abstract

A new series of salts $[RuCp(PP)(p\text{-}N{\equiv}C(CH{=}CH)_nC_6H_4R)][X]$ (PP = ((+)-DIOP, DPPE; $n = 0$, 1; R = CH_3, Br, OCH_3, NH_2, $N(CH_3)_2$, C_6H_5 and NO_2; X = PF_6^-, $CF_3SO_3^-$) were synthesised and the second harmonic generation (SHG) efficiencies were measured by Kurtz powder technique in order to better understand the relationship between structural features and solid state packing with SHG properties. A structural study of $[RuCp((+)\text{-DIOP})(p\text{-}N{\equiv}CC_6H_4NO_2)][X]$, X = PF_6^-, $CF_3SO_3^-$ by X-ray diffraction showed crystallisation on accentric groups. The PF_6^- salt crystallised in a triclinic space group $P1$ showing perfect parallel alignment of the molecular dipoles. The $CF_3SO_3^-$ salt crystallised in a monoclinic space group $P2_1$ and shows an angle of 73.8° between the molecular dipoles in the unit cell. Complex $[RuCp((+)\text{-DIOP})(p\text{-}N{\equiv}CCH_3)][PF_6]$, studied for comparison, crystallises in the $C222_1$ space group and shows eight molecules per unit cell randomly orientated. Comparison of the Ru–N and N≡C distances between the three compounds are in agreement with metal–nitrile bonding suggested by the spectroscopic data.

Keywords: NLO materials; Ruthenium; Nonlinear optics; Kurtz powder SHG; Crystal structures

1. Introduction

The exploitation of organometallic chemistry for the synthesis of new compounds with nonlinear optical (NLO) properties, motivated by relevance to optical device technology [1], has been during the past decade, a growing area of research [2,3]. The interest concerning the synthesis of organometallic compounds in view of their NLO properties was triggered by the publication of Green et al. [4] in 1987 concerning a ferrocene derivative, which was revealed to be 67 times more efficient than the urea standard, for the property of doubling the frequency of a Nd:YAG laser beam emitting at 1064 nm. This property of doubling frequencies is also known as second harmonic generation (SHG) and it is studied in solid materials by Kurtz powder technique (Kurtz powder SHG). Nonlinear optical properties of organometallic compounds have been explained by high molecular hyperpolarisability β origi-

* Corresponding author. Tel.: +351-21-8419317; fax: +351-21-8464455.
E-mail address: lena.garcia@ist.utl.pt (M. Helena Garcia).

0022-328X/01/$ - see front matter
PII: S0022-328X(01)01041-5

nated by strong charge transfer transitions occurring at the molecular level. Nevertheless, it has been found that molecules with high β values can present, at macroscopic level, vanishing Kurtz powder SHG values since this NLO property, measured in the solid state is strongly influenced by the crystal packing structure. Therefore, the necessary but not absolute criteria for a material to exhibit large second-order optical nonlinearity are that it should consist of polarisable dipolar molecules and that it should crystallise in a noncentrosymmetric space group. Molecular crystals built of a single enantiomer of a chiral compound necessarily exhibit a noncentrosymmetric structure although it does not ensure the lattice alignment of molecular dipoles required for optimised nonlinear properties.

Our strategy for the synthesis of organometallic compounds in view of the study of second order nonlinear optical properties in the solid state has been the use of chiral phosphines in the molecules of general formula $[M(\eta^5\text{-}C_5H_5)(PP)(p\text{-}N{\equiv}C(CH{=}CH)_nC_6H_4R)][PF_6]$ where M = Fe(II), Ru(II), PP is a bidentate phosphine and R is a donor or an acceptor group. Thus, we reported previously for $[FeCp((+)\text{-DIOP})(p\text{-}NCC_6H_4NO_2)][PF_6]$[1] [5] a Kurtz powder SHG efficiency of 38 times the urea standard and a value of ten times larger than urea for the ruthenium related compound $[RuCp((+)\text{-DIOP})(p\text{-}NCC_6H_4NO_2)][CF_3SO_3]$ [6]. The main feature of these structures is the location of the metal in the same plane as the conjugated π system improving their interaction. In fact, the significant values of the molecular hyperpolarisability β found for compounds of this family [7] was explained by the role of the iron and ruthenium monocyclopentadienyl moieties as very efficient donor groups towards the coordinated nitrile. In order to pursue the evaluation of the Kurtz powder SHG efficiencies of this general family of complexes, we systematically prepared several compounds of general formula $[RuCp((+)\text{-DIOP})(p\text{-}N{\equiv}C(CH{=}CH)_nC_6H_4R)][X]$ ($n = 0$, 1; R = CH_3, OCH_3, NH_2, NO_2, $N(CH_3)_2$, $C_6H_4NO_2$). Two different counter-ions, PF_6^- and $CF_3SO_3^-$, were used in order to influence the solid state packing. For the cationic complex $[RuCp(DPPE)(p\text{-}N{\equiv}CC_6H_4NO_2)]^+$ where the chiral coligand (+)-DIOP was substituted by the better σ-donor DPPE, the chiral counter-ion $C_4H_4O_7Sb^-$ was used with the aim of ensuring noncentrosymmetry. Finally the X-ray crystal structures of three relevant compounds were studied, namely compounds $[RuCp((+)\text{-DIOP})(p\text{-}NCC_6H_4NO_2)][PF_6]$, $[RuCp((+)\text{-DIOP}(p\text{-}NCC_6H_4NO_2)][CF_3SO_3]$ and $[RuCp((+)\text{-DIOP})(NCCH_3)][PF_6]$ in order to better understand the relationship between structural features and solid state packing with SHG property.

[1] (+)-DIOP = (+)-2,3-*O*-Isopropylidene-2,3-dihydroxy-1,4-bis-(diphenylphosphino)butane.

2. Results and discussion

2.1. Preparation of the complexes $[Ru(\eta^5\text{-}C_5H_5)(PP)(p\text{-}NCR)][X]$

Complexes of general formula $[Ru(\eta^5\text{-}C_5H_5)(PP)(p\text{-}NCR)][X]$ with PP = (+)-DIOP, $X = PF_6^-$: R = p-$C_6H_4CH_3$ (**1**), p-C_6H_4Br (**2**), p-$C_6H_4OCH_3$ (**3**), p-$C_6H_4NH_2$ (**4**), p-$C_6H_4N(CH_3)_2$ (**5**), (*E*)-p-CH=$CHC_6H_4NO_2$ (**6**), (*E*)-p-CH=$CHC_6H_4N(CH_3)_2$ (**7**), p-$C_6H_4C_6H_5$ (**8**), p-$C_6H_4C_6H_4NO_2$ (**9**), CH_3 (**10**); PP = (+)-DIOP, $X = CF_3SO_3^-$: R = p-C_6H_4F (**11**), (*E*)-p-CH=$CHC_6H_4NO_2$ (**12**), p-$C_6H_4C_6H_4NO_2$ (**13**) and $[Ru(\eta^5\text{-}C_5H_5)(DPPE)(p\text{-}NCC_6H_4NO_2)][C_4H_4O_7Sb]$ (**14**), were prepared by halide abstraction from the parent neutral complex $[Ru(\eta^5\text{-}C_5H_5)(PP)Cl]$ with a salt of the adequate counter-ion, in absolute methanol, in the presence of a slight excess of the corresponding nitrile. The reactions were carried out at room temperature, stirring overnight under inert atmosphere. The compounds were recrystallised from dichloromethane/diethylether or *n*-hexane, giving microcrystalline yellow greenish or orange products. With the exception of compound $[Ru(\eta^5\text{-}C_5H_5)(dppe)(p\text{-}NCC_6H_4NO_2)][C_4H_4O_7Sb]$ (**14**), which was hygroscopic and sensitive to moisture, all the compounds were fairly stable to air and moisture, either in the solid sate or in solution and were obtained in good yields of *ca.* 50–90%. The formulation is supported by analytical data, IR and ^{1}H-, ^{13}C-, ^{31}P-NMR spectroscopic data (see Section 4). The molar conductivities of *ca.* 10^{-3} M solutions of the complexes in nitromethane, in the range 72–102 $\Omega^{-1}\,cm^2\,mol^{-1}$ are consistent with the values reported for electrolytes 1:1 [8]. Typical bands confirm the presence of the cyclopentadienyl ligand ($\approx$3060 cm^{-1}), the PF_6^- anion (840 and 560 cm^{-1}), and the coordinated nitrile (ν_{CN} at $\approx$2220 cm^{-1}) in all the complexes studied. As observed before for other ruthenium analogous compounds, negative shifts up to -20 cm^{-1} were found on ν_{CN} by comparison with the uncoordinated nitrile. This effect has been attributed to π backdonation due to π bonding between the metal and the π^* orbital of the nitrile group which leads to a decreased N≡C bond order [6].

Chemical shifts of the cyclopentadienyl ring are displayed in the characteristic range of monocationic ruthenium(II) complexes and are insensitive to the electronic nature of the *p*-substituent on the coordinated nitrile, except in the case of *p*-nitro derivatives, for which a slight deshielding of 0.1 ppm was observed. The effect on coordination of the nitriles to the ruthenium(II) fragment is mainly found in the shielding observed in the protons directly bonded to the adjacent carbon of the NC group. Although in some cases this effect might be insignificant, a trend is clearly observed. The upfield shift of these protons indicates an electronic flow towards the aromatic protons due to a π-backdo-

nation effect involving the metal centre. These observed shifts are consistent with the possibility of some contribution of a vinylidene form in solution:

$$[Ru]^{+}–N{\equiv}C–C_6H_4–R \leftrightarrow [Ru]^{++}{=}N{=}C{=}C_6H_4{=}R^{-}$$

This effect was already found in our previous studies involving monocyclopentadienyliron(II) fragments containing bidentate phosphines [5,9].

^{13}C-NMR data of this family of compounds confirm the evidence found for proton spectra. Nevertheless, carbon resonances of cyclopentadienyl and nitrile aromatic backbone were revealed to be almost insensitive to coordination at the metal centre. The bidentate phosphine coligand presenting the signals of the carbon backbone in the corresponding ranges of the spectra showed to be insensitive to the nature of the aromatic nitrile.

^{31}P-NMR data of complexes reported in ppm downfield from the external standard (85% H_3PO_4) showed the presence of two doublets centred at 36 ppm indicating the nonequivalency of the two phosphorus atoms and the expected deshielding upon coordination of the phosphine in accordance with its σ donor character.

2.2. Electronic spectra

UV–vis electronic spectra of complexes [Ru(η^5-C_5H_5)(PP)(*p*-NCR)][X] were recorded in *ca.* 10^{-5} M solutions of methanol and chloroform, in the range 230–1100 nm (Table 1). All the spectra show two intense bands in the UV region at ≈210 and 360 nm with ε values in the range $1–3 \times 10^4$ M^{-1} cm^{-1}, characteristic of internal transitions on the aromatic ligands. In addition, a third band shows up in the region 300–400 nm with ε_{max} values in the range $1.3–3.7 \times 10^{-4}$ M. This transition was attributed to a metal to ligand charge transfer (MLCT) transition, since a comparable transition was absent either in [Ru(η^5-C_5H_5)((+)-DIOP)Cl] or in the uncoordinated nitrile chromophores. Accordingly, the dependence up to 77 nm on the position of λ_{max} depending on the polarity of the solvent was observed for some of the compounds. This behaviour is typified in Fig. 1, where the electronic spectrum of [Ru(η^5-C_5H_5)((+)-DIOP)(*p*-$NCC_6H_4C_6H_4NO_2$)][PF_6] (**9**), in methanol, is compared with the spectra of the parent ruthenium complex [Ru(η^5-C_5H_5)((+)-DIOP)-Cl] and the free nitrile *p*-$NCC_6H_4C_6H_4NO_2$.

2.3. Second order NLO characterisation

The efficiency of second harmonic generation (SHG) was measured using the Kurtz powder method [10]. All the measurements were performed at the Nd:YAG laser fundamental wavelength (1064 nm), due to the transparency of the samples at 532 nm, the second harmonic wavelength. Table 2 gathers the SHG relative efficien-

Table 1
UV–vis data for a family of compounds [Ru(η^5-C_5H_5)((+)-DIOP)(*p*-NCR)][PF_6]

Compound	[Ru(η^5-C_5H_5)((+)-DIOP)(*p*-NCR)][PF_6]	λ_{max} (nm) (ε, M^{-1} cm^{-1}) in chloroform		λ_{max} (nm) (ε, M^{-1} cm^{-1}) in methanol	
		Free nitrile	Complex	Free nitrile	Complex
1	R = $C_6H_4CH_3$		300 (10 900)		297 (13 500)
		268 (415)	273 (9600)	267 (718)	274 (sh)
		262 (sh)		232 (18 400)	
2	R = C_6H_4Br		311 (13 500)		310 (12 800)
		278 (436)		270 (sh)	249 (37 100)
				241 (23 500)	
3	R = $C_6H_4OCH_3$		295 (21 500)		294 (17 400)
		274 (sh)	275 (19 000)	248 (12 200)	250 (30 000)
4	R = $C_6H_4NH_2$		313 (21 500)		315 (36 500)
		269 (8800)	271 (10 700)	276 (24 600)	
				213 (13 700)	
6	R = $CH{=}CHC_6H_4NO_2$		387 (13 600)		310 (15 300)
		299 (18 500)	287 (26 300)	297 (27 700)	279 (32 100)
7	R = $CH{=}CHC_6H_4N(CH_3)_2$		411 (54 700)		401 (31 500)
		364 (33 500)	325 (8600)	362 (33 400)	319 (9200)
		331 (sh)		244 (10 400)	
8	R = $C_6H_4C_6H_5$		314 (18 300)		313 (sh)
		270 (23 900)	272 (20 500)	268 (22 500)	271 (19 700)
9	R = $C_6H_4C_6H_4NO_2$		335 (17 000)		380 (∼15 100)
		298 (11 000)	284 (30 200)	295 (26 000)	279 (∼18 000)
				243 (10 900)	
15	R = $C_6H_4NO_2$		385 (3200)		380 (2600)
		258 (12 700)	372 (10 500)	257 (24 700)	364 (7900)

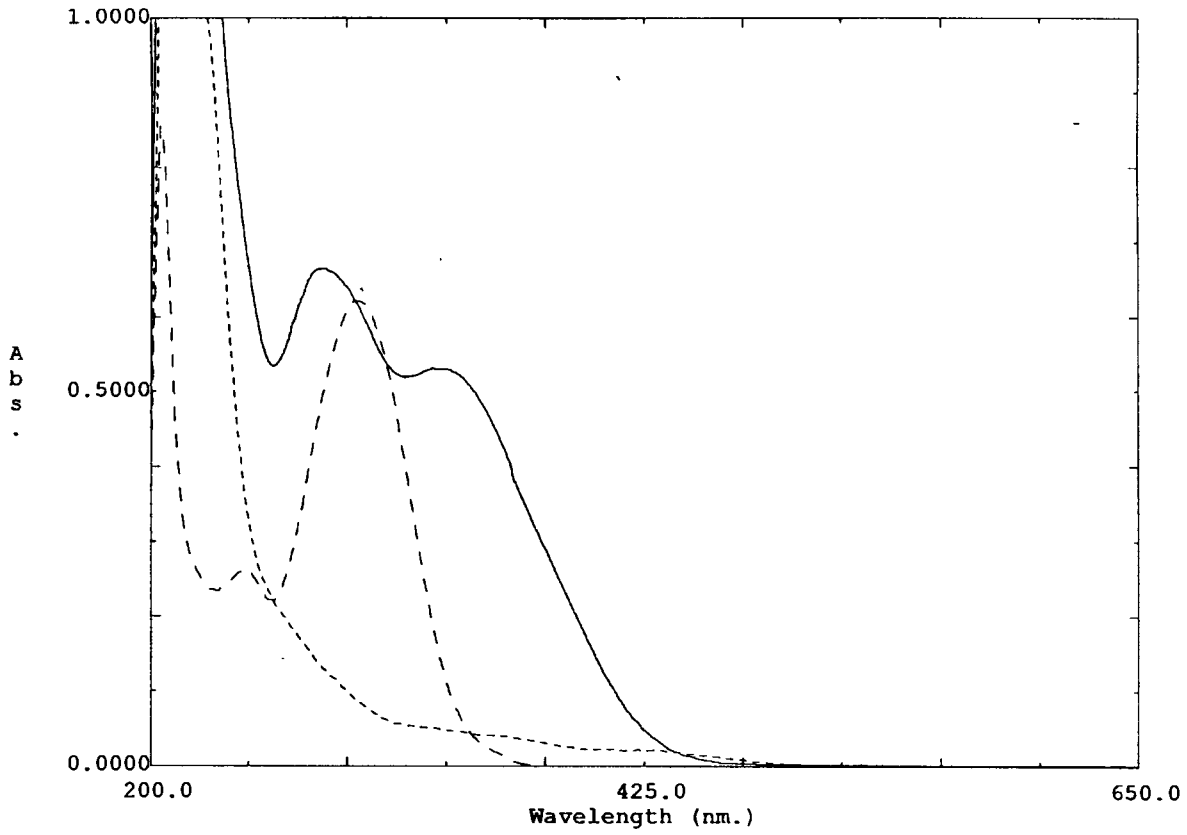

Fig. 1. Electronic spectra for $[Ru(\eta^5\text{-}C_5H_5)((+)\text{-DIOP})(p\text{-}NCC_6H_4C_6H_4NO_2)][PF_6]$ (**9**) (—), uncoordinated ligand (– – –) and starting material $[Ru(\eta^5\text{-}C_5H_5)((+)\text{-DIOP})(Cl)]$ (- - -) (*ca.* 5×10^{-5} M in methanol).

cies of the studied compounds together with the values obtained previously [6] for two additional compounds, derived from the most efficient chromophore *p*-$NCC_6H_4NO_2$, namely $[Ru(\eta^5\text{-}C_5H_5)((+)\text{-DIOP})(p\text{-}NCC_6H_4NO_2)][PF_6]$ (**15**) and $[Ru(\eta^5\text{-}C_5H_5)((+)\text{-DIOP})(p\text{-}NCC_6H_4NO_2)][CF_3SO_3]$ (**16**).

The best values of SHG are found for compounds possessing $R = NO_2$ group in the coordinated *p*-$NC(CH{=}CH)_nC_6H_4R$ nitriles, as would be expected. According to our earlier studies [5–7], the organometallic moiety [MCp(PP)]– (M = Fe(II) and Ru(II)) acting as a π donor via d–π* (NC) orbitals towards the NO_2 acceptor group enhances the hyperpolarisability of the coordinated nitrile giving rise to a large molecular second order hyperpolarisability which is related to nonlinear optical properties. However, it is important to stress that results obtained with the Kurtz powder technique are very difficult to interpret in terms of molecular structure–property relationships, since they depend not only on the molecular hyperpolarisability β, but also very strongly on the crystal packing structure, grain size, phase-matching properties, etc. Having this in mind, and considering that our set of results is affected by the same experimental errors, a very qualitative comparison of the SHG values shows for the coordinated nitriles the following trend: *p*-$NCC_6H_4NO_2$ (**15** and **16**) > (*E*)-*p*-$NCCH{=}CHC_6H_4NO_2$ (**6** and **12**) > *p*-$NCC_6H_4C_6H_4NO_2$ (**9** and **13**), which suggests that the introduction of the *trans*-ethenyl group in the *p*-benzonitrile ligand is more efficient than the introduction

Table 2
Evaluation of SHG for compounds $[Ru(\eta^5\text{-}C_5H_5)(PP)(p\text{-}NCR)][X]$

Compound $[Ru(\eta^5\text{-}C_5H_5)(PP)(p\text{-}NCR)][X]$	SHG value [a]
PP = (+)-DIOP, X = PF_6^-	
R = *p*-$C_6H_4CH_3$ (**1**)	0.00
R = *p*-$C_6H_4OCH_3$ (**3**)	0.03
R = *p*-$C_6H_4NH_2$ (**4**)	0.00
R = (*E*)-*p*-$CH{=}CHC_6H_4NO_2$ (**6**)	1.96
R = (*E*)-*p*-$CH{=}CHC_6H_4N(CH_3)_2$ (**7**)	0.40
R = *p*-$C_6H_4NO_2$ (**15**)	2.66 [b]
R = *p*-$C_6H_4C_6H_4NO_2$ (**9**)	0.82
PP = (+)-DIOP, X = $CF_3SO_3^-$	
R = *p*-C_6H_4F (**11**)	0.00
R = *p*-$C_6H_4NO_2$ (**16**)	10.0 [b]
R = (*E*)-*p*-$CH{=}CHC_6H_4NO_2$ (**12**)	1.20
R = *p*-$C_6H_4C_6H_4NO_2$ (**13**)	0.80
PP = DPPE, X = $C_4H_4O_7Sb^-$	
R = *p*-$C_6H_4NO_2$ (**14**)	0.0

[a] Second harmonic intensity measured at 1.064 μm fundamental radiation, relative to urea.
[b] Ref. [6].

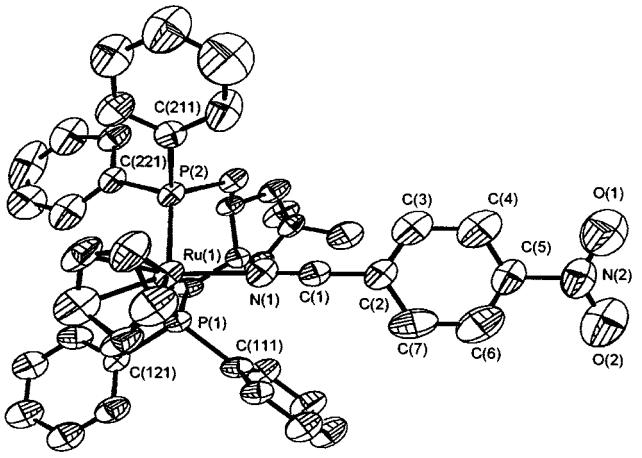

Fig. 2. ORTEP diagram for $[Ru(\eta^5\text{-}C_5H_5)((+)\text{-DIOP})(p\text{-}NCC_6H_4NO_2)][PF_6]$ (**15**), with 40% thermal ellipsoids, showing the labelling scheme. Hydrogen atoms have been omitted for clarity.

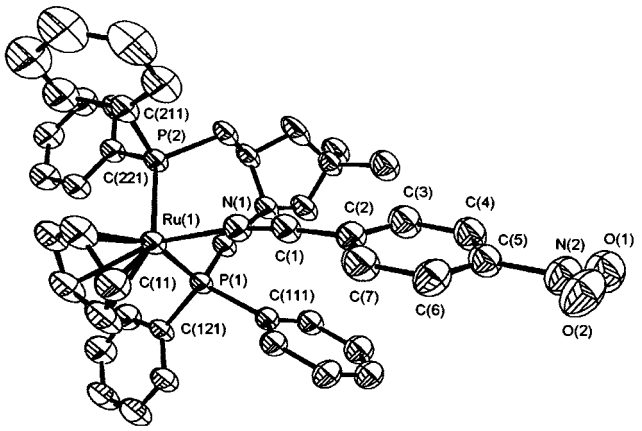

Fig. 3. ORTEP diagram for $[Ru(\eta^5\text{-}C_5H_5)((+)\text{-DIOP})(p\text{-}NCC_6H_4NO_2)][CF_3SO_3]\cdot C_2H_5OC_2H_5$ (**16**), with 40% thermal ellipsoids, showing the labelling scheme. Hydrogen atoms have been omitted for clarity.

of one phenyl group. This is not surprising since planarity will be better preserved for the case of one *trans*-ethenyl group. This observed trend is in good agreement with the results of the molecular hyperpolarisabilities β measured for the analogous compounds possessing the chromophores $p\text{-}NCC_6H_4NO_2$ and $p\text{-}NCC_6H_4C_6H_4NO_2$, namely $[Ru(\eta^5\text{-}C_5H_5)(DPPE)(p\text{-}NCC_6H_4NO_2)][PF_6]$ and $[Ru(\eta^5\text{-}C_5H_5)(DPPE)\text{-}(p\text{-}NCC_6H_4C_6H_4NO_2)][PF_6]$ which were 138 and 96×10^{-30} esu, respectively [7].

Although it is well known that the effect of the counter-ion is an important contributing factor for the solid state packing, these results do not suggest any pattern which allows the choice of any favourable anion. In fact, the effect of PF_6^- and $CF_3SO_3^-$ on the SHG values of compounds **6** and **12** is reversed when we compare **15** and **16**. The same conclusion can be drawn when analogous Fe(II) and Ru(II) compounds are compared [5,6]. Surprisingly, compound $[Ru(\eta^5\text{-}C_5H_5)(DPPE)p\text{-}NCC_6H_4NO_2][C_4H_4O_7Sb]$ is ineffective on SHG property in spite of the expected accentric crystallisation due to the presence of the chiral $C_4H_4O_7Sb^-$ anion.

2.4. Crystallographic studies

X-ray crystal structures of two compounds derived from the same chromophore and crystallised with two different counter-ions were studied with the aim of better understanding the relationship between the solid state packing and the SHG property. A third compound possessing the same ruthenium moiety with the acetonitrile ligand in the place of chromophore was studied for comparison of atomic distances and to better understand the chemical bonding and possible solid state interactions.

The molecular structures of $[RuCp((+)DIOP)(p\text{-}NCC_6H_4NO_2)][PF_6]$ (**15**), $[RuCp((+)DIOP)(p\text{-}NCC_6H_4NO_2)][CF_3SO_3]\cdot C_2H_5OC_2H_5$ (**16**) and $[RuCp\text{-}((+)\text{-}DIOP)(NCCH_3)][PF_6]$ (**10**) are presented in Figs. 2–4, along with the atomic numbering scheme. Selected bond lengths and bond angles are given in Table 3.

In all compounds, the metal is coordinated to the η^5-cyclopentadienyl ring, the two phosphorus atoms of the phosphine ligand and a nitrogen atom (the nitrile nitrogen atom of the $p\text{-}NCC_6H_4NO_2$ ligand for **15** and **16** and the nitrogen atom of the acetonitrile ligand for **10**), showing the typical structure of cyclopentadienyl complexes in a pseudo-octahedral three-legged piano stool geometry, on the assumption that the cyclopentadienyl group takes up three coordination sites. This pseudo-octahedral geometry is confirmed by the N–Ru–P and P–Ru–P angles around the ruthenium

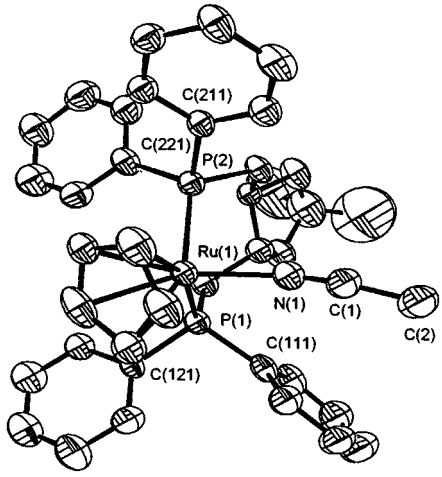

Fig. 4. ORTEP diagram for $[Ru(\eta^5\text{-}C_5H_5)((+)\text{-DIOP})(NCCH_3)][PF_6]$ (**10**), with 40% thermal ellipsoids, showing the labelling scheme. Hydrogen atoms have been omitted for clarity.

Table 3
Values of selected bond lengths (Å) and bond angles (°) for [RuCp((+)-DIOP)(*p*-$NCC_6H_4NO_2$)][PF_6] (**15**), [RuCp((+)-DIOP)(*p*-$NCC_6H_4NO_2$)][CF_3SO_3]·$C_2H_5OC_2H_5$ (**16**) and [RuCp((+)-DIOP)($NCCH_3$)][PF_6] (**10**)

	15	**16**	**10**
Ru(1)–P(1)	2.330(4)	2.3030(15)	2.303(4)
Ru(1)–P(2)	2.309(4)	2.3124(16)	2.296(3)
Ru(1)–N(1)	2.031(13)	2.030(5)	2.047(14)
N(1)–C(1)	1.137(18)	1.130(8)	1.088(18)
C(1)–C(2)	1.42(2)	1.440(9)	1.48(2)
C(2)–C(3)	1.36(2)	1.388(10)	
C(3)–C(4)	1.43(2)	1.379(11)	
C(4)–C(5)	1.34(3)	1.348(11)	
C(5)–C(6)	1.33(3)	1.351(12)	
C(6)–C(7)	1.40(2)	1.400(11)	
C(2)–C(7)	1.38(2)	1.379(10)	
C(5)–N(2)	1.50(2)	1.471(10)	
N(2)–O(1)	1.27(3)	1.232(11)	
N(2)–O(2)	1.20(2)	1.210(11)	
Ru(1)–N(1)–C(1)	177.2(12)	168.9(5)	169.8(13)
N(1)–C(1)–C(2)	178.6(15)	173.1(7)	173(2)
P(2)–Ru(1)–P(1)	96.48(12)	97.57(6)	98.92(15)
N(1)–Ru(1)–P(1)	89.5(4)	89.72(16)	88.7(4)
N(1)–Ru(1)–P(2)	89.9(4)	89.11(16)	90.4(3)
C(η^5-centroid)–Ru(1)–N(1)	124.0(9)	123.6(4)	123.9(9)
C(η^5-centroid)–Ru(1)–P(1)	124.1(10)	124.1(3)	125.1(7)
C(η^5-centroid)–Ru(1)–P(2)	123.3(10)	123.3(3)	123.3(6)

atom, which are all close 90° for the three complexes and the remaining Cp(η^5-centroid)–Ru–X (with X = N, P) angles which are around 120° (see Table 3).

In the three compounds, the phosphine adopts a twisted chair conformation and the Ru–P bond lengths (see Table 3) are similar to other RuDIOP complexes found in the Cambridge Structural Data Base [11] that have Ru–P bond distances ranging from 2.247 to 2.393 Å.

A comparison between the parameters defining the geometry of the nitriles bonded to the Ru atom is given in Table 4 for the reported structures of [$RuCpL_2L'$] (L = PPh_3; L′ = $NCC(CN)_2$, $NC(C_6H_4)OC_2H_5$, $NC(CH_3)$) complexes containing Ru–P or Ru–N≡C bonds.

The Ru–N bond lengths in the three compounds, in the range 2.030(5)–2.047(14) Å, are similar and comparable to the other ruthenium(II) complexes referred in Table 4, except to the bond distance Ru–N of the compound [$RuCp(PPh_3)_2(NCC(CN)_2)$]·CH_2Cl_2 [12] where the value found is larger. The N–C bond lengths for the three studied compounds with the values 1.137(18), 1.130(8) and 1.088(18) Å are in good agreement with the existence of π-backdonation suggested by the IR and NMR spectroscopic data for compounds **15** and **16**. Nevertheless, this π-backdonation effect is not extended through the benzene ring since distances and angles within the benzonitrile group (in compounds **15** and **16**) are consistent with the retention of aromaticity. In fact, there is no obvious bond length alternation which would be expected for appreciable quinoidal contribution.

In complex **15** the nitrile group shows an almost linear geometry with Ru–N1–C1 and N1–C1–C2 angles of 177.2(12) and 178.6(15)°, respectively, which indicate that the ruthenium atom and the benzonitrile ligand are in the same plane that could stimulate the metal–ligand π-backdonation. As for complexes **16** and **10** the nitrile group deviates somewhat from linear geometry since the angles Ru–N1–C1 and N1–C1–C2 are 168.9(5) and 173.1(7)° for complex **16** and 169.8(13) and 173(2)° for complex **10**.

The focus of this work being the optical nonlinearities of the nitrile complexes, it seems relevant to examine the crystal packing as an indicator of bulk material response. In view of NLO properties, such as SHG, the most decisive feature revealed by the crystal structure is the relative position of the molecules in the lattice. All these studied complexes crystallise in noncentrosymmetric space groups as would be expected due to the presence of the chiral phosphine coligand (+)-DIOP.

Fig. 5 shows the crystal packing diagram of complex **15** along the crystallographic *a*-axis, providing a clear view of the compound in the solid state. The crystal packing in the triclinic space group *P*1, with one independent molecule in the unit cell, shows that there is a perfect parallel alignment of the molecular dipoles. As can be seen, the supramolecular alignment of the complex molecules is stabilised by three relatively weak and independent C–H···O hydrogen bonding interactions. We can observe one hydrogen interaction between the

Table 4
Structural data for $[CpRu(PP)]^+$ derivatives containing nitrile ligands

Compound	Ru–N (Å)	N≡C (Å)	Ru–N–C (°)	N–C–C (°)	Ref.
[$RuCp(PPh_3)_2NCC(CN)_2$]·CH_2Cl_2	2.072(5)	1.137(9)	173.7(6)		[12]
[$RuCp(PPh_3)_2NCPhOEt$][PF_6]	2.041(5)	1.152 [a]	175.6 [a]	175.1 [a]	[26]
[$RuCp(PPh_3)_2NCCH_3$][BF_4]	2.040(3)	1.129(6)	169.8(5)	178.8 [a]	[27]
[RuCp(DIOP)(*p*-$NCC_6H_4NO_2$)][PF_6]	2.031(13)	1.137(18)	177.2(12)	178.6(15)	This work
[RuCp((+)-DIOP)(*p*-$NCC_6H_4NO_2$)][CF_3SO_3]·$C_2H_5OC_2H_5$	2.030(5)	1.130(8)	168.9(5)	173.1(7)	This work
[RuCp(DIOP)($NCCH_3$)][PF_6]	2.047(14)	1.088(18)	169.8(13)	173(2)	This work

[a] Values taken from Cambridge Data Base [11].

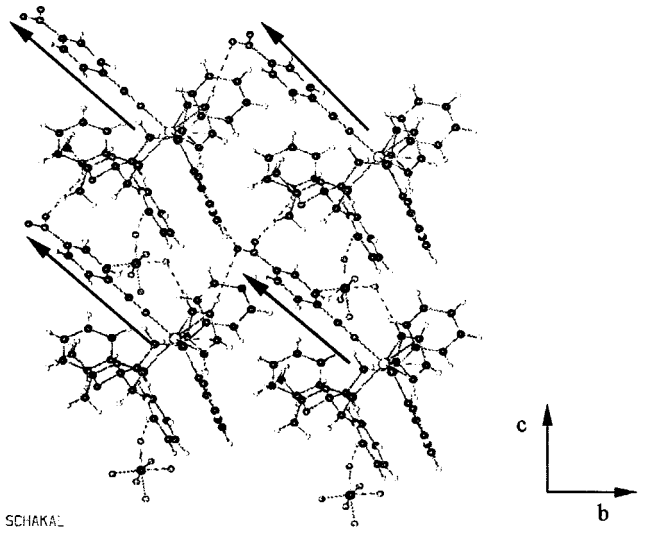

Fig. 5. Crystal packing for [Ru(η^5-C_5H_5)((+)-DIOP)(*p*-$NCC_6H_4NO_2$)][PF_6] (**15**).

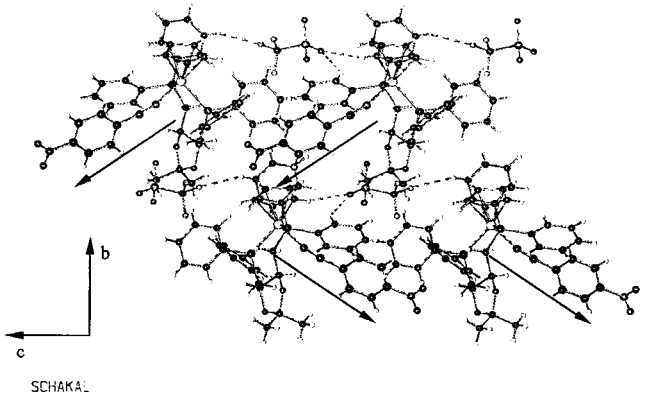

Fig. 6. Crystal packing for [Ru(η^5-C_5H_5)((+)-DIOP)(*p*-$NCC_6H_4NO_2$)][CF_3SO_3]·$C_2H_5OC_2H_5$ (**16**).

oxygen atom of the nitro group O(2) and an hydrogen of the Cp ring of one neighbouring cation molecule in the same layer (C(12) – H(12)···O(2), 2.82(3) Å) and a second interaction between the O(1) and an aromatic hydrogen of one phosphine phenyl ring of another neighbouring cation in the same layer (C(116) – H(116)···O(1), 2.73(4) Å). These two hydrogen bonds will extend the 1D alignment along the *c* crystallographic direction. The third hydrogen interaction, between the O(2) and the phosphine aromatic hydrogen belonging to a cationic molecule from a neighbouring layer (C(225) – H(225)···O(2), 2.66(4) Å) connects the cationic units also along the *b* axis and is also responsible for the global alignment.

The crystal packing is also reinforced by short C – H···F hydrogen bonding interactions (in the order of 2.48 and 2.50 Å), that are responsible for the hydrogen bonding between the cations and the anions, this keeping together cations of different layers. Each PF_6^- holds together two cations from different layers, namely C – H(3)···F(2) and C – H(11)···F(6) from the same molecule in one layer and C – H(125)···F(1) from a cationic molecule in another layer.

[RuCp((+)-DIOP)(*p*-$NCC_6H_4NO_2$)][CF_3SO_3]·$C_2H_5OC_2H_5$ (**16**) crystallises in the monoclinic space group $P2_1$ with two independent molecules in the unit cell. A view of the crystal packing of this complex along the *a* axis is presented in Fig. 6 showing that the angle between the planes of the nitrile ligands of each independent molecule is 73.8°.

This crystal packing is stabilised by some hydrogen bond interactions between the cations and the anions and also the cations and the solvent molecules. Each $CF_3SO_3^-$ anion holds together two cations molecules of different layers, C – H(116)···O(41) (2.62(3) Å), C – H(11)···O(41) (2.53(5) Å), from one molecule and C – H(125)···F(42) (2.54(4) Å) from another molecule along the *c* axis. The solvent molecules were omitted for clarity from the crystal packing (Fig. 6), although there exists one interaction between the cation and the solvent molecule connecting the cation molecules along the *a* axis (C – H(125)···O(51), 2.61(4) Å).

Comparison of the solid state packing of these two compounds, containing the same chromophore and crystallised with two different counter-ions (Figs. 5 and 6), shows that the introduction of a larger and not so symmetric counter-ion, $CF_3SO_3^-$, disrupts the perfect alignment of the cationic molecules found for compound **15** crystallised with the PF_6^- anion.

For second harmonic generation purposes, the precise orientation of the molecules in the crystal plays an important role and more important than the perfect alignment of all the dipoles, is the angle between the molecular charge transfer axis (typically along the donor–acceptor axis) and the polar crystal axis. The optimum value of this angle was found to depend on the crystal space group, in order to allow quadratic phase-matched interactions [13–15]. In complex **15** this angle is 83.5° and in **16** is 70.3°, both far from the optimum values of 35.26° (for space group $P1$) and 54.74° (for space group $P2_1$) [16].

The significant deviation from the optimal phase-matching direction, namely 44.74° (**15**) and 28.76° (**16**), explains the relatively small SHG values found for these compounds and also the poorer value of **15** when compared with **16**. Nevertheless, comparisons must be made with caution since these crude measurements did not account for fluorescence and grain size of the samples.

3. Concluding remarks

SHG Kurtz powder technique was used as an expeditious method to screen compounds for NLO purposes.

On the basis of the SHG Kurtz efficiencies and crystal packing structures of compounds **15** and **16**, it can be expected that studies on the variation of the counter-ion leading to better phase-matching conditions can therefore improve the SHG values for these compounds.

4. Experimental

4.1. General procedures

All the experiments were carried out under vacuum or dinitrogen atmosphere using standard Schlenk techniques. All the solvents used were dried following standard methods [17]. Absolute MeOH was used without further purification and degassed before use. Starting materials [Ru(η^5-C_5H_5)(PP)Cl] (PP = (+)-DIOP and DPPE) were prepared following methods described in the literature [18]. IR spectra were recorded on a Perkin–Elmer 683 spectrophotometer with KBr pellets; only significant bands are cited in the text. ^{1}H-, ^{13}C-, and ^{31}P-NMR spectra were recorded on a Varian Unity 300 spectrometer at probe temperature. The ^{1}H (Me_2CO-d_6) and ^{13}C ($CHCl_3$-*d*) chemical shifts are reported in parts per million (ppm) downfield from internal Me_4Si and the ^{31}P ($CHCl_3$-*d*) NMR spectra are reported in ppm downfield from external standard, 85% H_3PO_4. The molar conductivities of 10^{-3} mol l^{-1} solutions of the complexes in nitromethane were recorded with a Schott CGB55 Konduktometer. Elemental analyses were obtained at Laboratório de Análises, Instituto Superior Técnico, using a Fisons Instruments EA1108 system. Data acquisition, integration and handling were performed using a PC with the software package EAGER-200 (Carlo Erba Instruments). Melting points were obtained on a Reichert Thermovar equipment.

^{1}H- and ^{13}C-NMR data relative to (+)-DIOP coordinated phosphine, described here for compound [Ru(η^5-C_5H_5)((+)-DIOP)(p-$NCC_6H_4CH_3$)][PF_6] (**1**), are very similar in all compounds: ^{1}H (Me_2CO-d_6): 1.06 (s, 3H, CH_3); 1.26 (s, 3H, CH_3); 2.59 (m, 1H, CH); 3.00 (m, 1H, CH); 3.40 (m, 2H, CH_2); 3.80 (m, 2H, CH_2); 7.46 (m, 10H, C_6H_5); 7.65 (m, 4H, C_6H_5); 7.78 (m, 4H, C_6H_5); 8.12 (t, 2H, C_6H_5). ^{13}C{^{1}H}-NMR ($CDCl_3$): 26.75 (CH_3); 28.73 (CH_2, ^1J(C–P) = 20.49 Hz); 30.48 (CH_2, ^1J(C–P) = 26.85 Hz); 75.42 (CH, ^2J(C–P) = 10.40 Hz); 78.23 (CH), 108.90 ($C(CH_3)_2$); 128.92–134.16 (aryl-CH); 138.38 (C-*ipso*, aryl-CH); 141.27 (C-*ipso*, aryl-CH).

4.2. Preparation of [Ru(η^5-C_5H_5)((+)-DIOP)(p-NCR)][PF_6]

Complexes [Ru(η^5-C_5H_5)((+)-DIOP)(*p*-NCR)][PF_6] were prepared by halide abstraction of [Ru(η^5-C_5H_5)(PP)Cl] (1 mmol) with $TlPF_6$ (1 mmol) in absolute MeOH, in presence of the slight excess of adequate nitrile (1.1 mmol), at room temperature (r.t.), stirring overnight for 18 h under an inert atmosphere. After work-up the compounds were recrystallised from CH_2Cl_2–Et_2O or *n*-hexane, giving microcrystalline products, mostly yellow greenish.

4.2.1. [Ru(η^5-C_5H_5)((+)-DIOP)(p-$NCC_6H_4CH_3$)][PF_6] (1)

Yellow; recrystallised from CH_2Cl_2–*n*-hexane; 88% yield; m.p. 130–132 °C; molar conductivity = 74.0 Ω^{-1} cm^2 mol^{-1}. IR (KBr, cm^{-1}): *v*(CN) 2220. ^{1}H-NMR (Me_2CO-d_6): 2.43 (s, 3H, CH_3); 4.58 (s, 5H, η^5-C_5H_5); 7.33 (d, 2H, H_3, H_5); 7.40 (d, 2H, H_2, H_6). ^{13}C{^{1}H}-NMR ($CDCl_3$): 21.94 (CH_3); 83.55 (C_5H_5); 107.51 (C1); 128.76–134.32 (C3, C5, CN, C2, C6 + Ph); 145.42 (C4). ^{31}P{^{1}H}-NMR ($CDCl_3$): 36.3 (2d, $J(P_AP_B)$ = 38.2 Hz). Anal. Found: C, 55.63; H, 4.87; N, 1.51. Calc. for $C_{44}H_{44}F_6NO_2P_3Ru \cdot 1/2CH_2Cl_2$: C, 55.14; H, 4.68; N, 1.44%.

4.2.2. [Ru(η^5-C_5H_5)((+)-DIOP)(p-NCC_6H_4Br)][PF_6] (2)

Yellow greenish; recrystallised from CH_2Cl_2–*n*-hexane; 70% yield; m.p. 201–204 °C; molar conductivity = 76.7 Ω^{-1} cm^2 mol^{-1}. IR (KBr, cm^{-1}): *v*(CN) 2230. ^{1}H-NMR (Me_2CO-d_6): 4.61 (s, 5H, η^5-C_5H_5); 7.36–7.81 (m, 4H + Ph, H_3, H_5, H_2, H_6). ^{13}C{^{1}H}-NMR ($CDCl_3$): 83.84 (C_5H_5); 108.87 (C1); 128.29 (C4); 130.03 (CN); 131.26 (C3, C5); 132.62 (C2, C6). ^{31}P{^{1}H}-NMR ($CDCl_3$): 36.2 (2d, $J(P_AP_B)$ = 36.4 Hz). Anal. Found: C, 51.90; H, 4.17; N, 1.43. Calc. for $C_{43}H_{41}BrF_6NO_2P_3Ru$: C, 52.08; H, 4.17; N, 1.41%.

4.2.3. [Ru(η^5-C_5H_5)((+)-DIOP)(p-$NCC_6H_4OCH_3$)][PF_6] (3)

Yellow; recrystallised from CH_2Cl_2–Et_2O; 60% yield; m.p. 206–209 °C; molar conductivity = 94.7 Ω^{-1} cm^2 mol^{-1}. IR (KBr, cm^{-1}): *v*(CN) 2220, *v*(OCH_3) 1260. ^{1}H-NMR (Me_2CO-d_6): 3.90 (s, 3H, OCH_3); 4.57 (s, 5H, η^5-C_5H_5); 7.10 (d, 2H, H_3, H_5); 7.39 (d, 2H, H_2, H_6). ^{13}C{^{1}H}-NMR ($CDCl_3$): 55.77 (OCH_3); 83.40 (C_5H_5); 101.81 (C1); 115.24 (C3, C5); 130.14 (CN); 134.28 (C2, C6); 163.90 (C4). ^{31}P{^{1}H}-NMR ($CDCl_3$): 36.1 (2d, $J(P_AP_B)$ = 38.2 Hz). Anal. Found: C, 55.67; H, 4.71; N, 1.48. Calc. for $C_{44}H_{44}F_6NO_3P_3Ru$: C, 56.05; H, 4.70; N, 1.51%.

4.2.4. [Ru(η^5-C_5H_5)((+)-DIOP)(p-$NCC_6H_4NH_2$)][PF_6] (4)

Yellow; recrystallised from CH_2Cl_2–*n*-hexane; 57% yield; m.p. 173 °C; molar conductivity = 93.3 Ω^{-1} cm^2 mol^{-1}. IR (KBr, cm^{-1}): *v*(NH_2) 3500, 3400,

ν(CN) 2220. ^{1}H-NMR (Me_2CO-d_6): 4.52 (s, 5H, η^5-C_5H_5); 5.93 (br, 2H, NH_2); 6.71 (d, 2H, H_3, H_5); 7.07 (d, 2H, H_2, H_6). $^{13}C\{^1H\}$-NMR ($CDCl_3$): 83.02 (C_5H_5); 96.17 (C1); 114.54 (C3, C5); 130.35 (CN); 133.67 (C2, C6); 152.58 (C4). $^{31}P\{^1H\}$-NMR ($CDCl_3$): 36.2 (2d, $J(P_AP_B) = 38.2$ Hz). Anal. Found: C, 53.11; H, 4.56; N, 2.88. Calc. for $C_{43}H_{43}F_6N_2O_2P_3Ru \cdot 1/2CH_2Cl_2$: C, 53.85; H, 4.57; N, 2.89%.

4.2.5. [Ru(η^5-C_5H_5)((+)-DIOP)-(p-$NCC_6H_4N(CH_3)_2$)][PF_6] (5)

Yellow greenish; recrystallised from CH_2Cl_2–Et_2O; 80% yield; m.p. 185–190 °C; molar conductivity = 72.0 Ω^{-1} cm^2 mol^{-1}. IR (KBr, cm^{-1}): $\nu(N(CH_3)_2)$ 2950, ν(CN) 2220. ^{1}H-NMR (Me_2CO-d_6): 3.08 (s, 6H, $N(CH_3)_2$); 4.52 (s, 5H, η^5-C_5H_5); 6.75 (d, 2H, H_3, H_5); 7.19 (d, 2H, H_2, H_6). $^{13}C\{^1H\}$-NMR ($CDCl_3$): 39.87 ($N(CH_3)_2$); 83.17 (C_5H_5); 94.53 (C1); 111.62 (C3, C5); 131.71 (CN), 133.46 (C2, C6); 153.20 (C4). $^{31}P\{^1H\}$-NMR ($CDCl_3$): 36.5 (2d, $J(P_AP_B) = 38.2$ Hz). Anal. Found: C, 55.95; H, 5.20; N, 2.98. Calc. for $C_{45}H_{47}F_6N_2O_2P_3Ru$: C, 56.54; H, 4.96; N, 2.93%.

4.2.6. [Ru(η^5-C_5H_5)((+)-DIOP)-((E)-p-NCCH=$CHC_6H_4NO_2$)][PF_6] (6)

Orange; recrystallised from CH_2Cl_2–Et_2O; 80% yield; m.p. 194 °C; molar conductivity = 101.8 Ω^{-1} cm^2 mol^{-1}. IR (KBr, cm^{-1}): ν(CN) 2225, ν(CH=CH) 1610, $\nu(NO_2)$ 1520, 1340. ^{1}H-NMR (Me_2CO-d_6): 4.57 (s, 5H, η^5-C_5H_5); 6.82 (d, 1H, H_8, $^1J_{HH} = 16.5$ Hz); 7.07 (d, 1H, H_7, $^1J_{HH} = 16.5$ Hz); 7.83 (d, 2H, H_2, H_6); 8.29 (d, 2H, H_3, H_5). $^{13}C\{^1H\}$-NMR ($CDCl_3$): 83.82 (C_5H_5); 100.33 (C8); 124.18 (C3, C5); 128.19 (CN); 128.60–134.25 (C2, C6 + Ph); 138.91 (C1); 148.98 (C4); 149.34 (C7). $^{31}P\{^1H\}$-NMR ($CDCl_3$): 36.1 (2d, $J(P_AP_B) = 38.2$ Hz). Anal. Found: C, 53.48; H, 4.57; N, 2.91. Calc. for $C_{45}H_{43}F_6N_2O_4P_3Ru \cdot 1/2CH_2Cl_2$: C, 53.25; H, 4.32; N, 2.73%.

4.2.7. [Ru(η^5-C_5H_5)((+)-DIOP)-((E)-p-NCCH=$CHC_6H_4N(CH_3)_2$)][PF_6] (7)

Dark green; recrystallised from CH_2Cl_2–n-hexane; 58% yield; m.p. 236–239 °C; molar conductivity = 76.6 Ω^{-1} cm^2 mol^{-1}. IR (KBr, cm^{-1}): ν(CN) 2210, ν(CH=CH) 1610. ^{1}H-NMR (Me_2CO-d_6): 3.07 (s, 6H, $N(CH_3)_2$); 4.51 (s, 5H, η^5-C_5H_5); 6.08 (d, 1H, H_8, $^1J_{HH} = 16.5$ Hz); 6.63 (d, 1H, H_7, $^1J_{HH} = 15.9$ Hz); 6.73 (d, 2H, H_3, H_5); 7.34 (d, 2H, H_2, H_6). $^{13}C\{^1H\}$-NMR ($CDCl_3$): 39.97 ($N(CH_3)_2$); 83.23 (C_5H_5); 87.21 (C8); 111.60 (C3, C5); 120.77 (C1); 128.78 (C2, C6); 130.55 (CN); 152.77 (C4); 152.77 (C7). $^{31}P\{^1H\}$-NMR ($CDCl_3$): 36.4 (2d, $J(P_AP_B) = 38.2$ Hz). Anal. Found: C, 57.56; H, 5.12; N, 2.86. Calc. for $C_{47}H_{49}F_6N_2O_2P_3Ru$: C, 57.49; H, 5.03; N, 2.85%.

4.2.8. [Ru(η^5-C_5H_5)((+)-DIOP)(p-$NCC_6H_4C_6H_5$)][PF_6] (8)

Yellow greenish; recrystallised from CH_2Cl_2–Et_2O; 90% yield; m.p. 171–174 °C; molar conductivity = 90.4 Ω^{-1} cm^2 mol^{-1}. IR (KBr, cm^{-1}): ν(CN) 2220. ^{1}H-NMR (Me_2CO-d_6): 4.60 (s, 5H, η^5-C_5H_5); 7.35–8.08 (m, 9H + Ph, H_2, H_{12}, H_3, H_{11}, H_6, H_{10}, H_7, H_8, H_9). $^{13}C\{^1H\}$-NMR (Me_2CO-d_6): 84.54 (C_5H_5); 110.56 (C1); 128.04 (C7, C8, C9); 128.59 (C3, C11, C6, C10); 126.68 (CN); 133.85 (C2, C12); 139.35 (C4); 147.22 (C5). $^{31}P\{^1H\}$-NMR ($CDCl_3$): 36.3 (2d, $J(P_AP_B) = 37.5$ Hz). Anal. Found: C, 59.47; H, 4.92; N, 1.23. Calc. for $C_{49}H_{46}F_6NO_2P_3Ru \cdot 0.5CH_2Cl_2$: C, 59.70; H, 5.01; N, 1.36%.

4.2.9. [Ru(η^5-C_5H_5)((+)-DIOP)-(p-$NCC_6H_4C_6H_4NO_2$)][PF_6] (9)

Yellow greenish; recrystallised from CH_2Cl_2–Et_2O; 85% yield; m.p. 230 °C; molar conductivity = 86.2 Ω^{-1} cm^2 mol^{-1}; IR (KBr, cm^{-1}): ν(CN) 2220, $\nu(NO_2)$ 1515, 1345. ^{1}H-NMR (Me_2CO-d_6): 4.63 (s, 5H, η^5-C_5H_5); 7.60 (d, 2H, H_2, H_{12}); 8.04 (2d, 4H, H_3, H_{11}, H_6, H_{10}); 8.37 (d, 2H, H_7, H_9). $^{13}C\{^1H\}$-NMR (Me_2CO-d_6): 84.54 (C_5H_5); 110.56 (C1); 128.04 (C7, C8, C9); 128.59 (C3, C11, C6, C10); 126.68 (CN); 133.85 (C2, C12); 139.35 (C4); 147.22 (C5). $^{31}P\{^1H\}$-NMR ($CDCl_3$): 36.1 (2d, $J(P_AP_B) = 38.2$ Hz). Anal. Found: C, 56.63; H, 4.40; N, 2.71. Calc. for $C_{49}H_{45}F_6N_2O_4P_3Ru$: C, 56.92; H, 4.39; N, 2.71%.

4.2.10. [Ru(η^5-C_5H_5)((+)-DIOP)($NCCH_3$)][PF_6] (10)

Green; recrystallised from Me_2CO–Et_2O. IR (KBr, cm^{-1}): ν(CN) 2190. ^{1}H-NMR (Me_2CO-d_6): 2. 43 (s, 3H, CH_3); 4.44 (s, 5H, η^5-C_5H_5). Anal. Found: C, 53.68; H, 4.74; N, 1.71. Calc. for $C_{38}H_{40}F_6NO_2P_3Ru$: C, 53.65; H, 4.74; N, 1.65%.

4.2.11. Ru(η^5-C_5H_5)((+)-DIOP)-(p-NCC_6H_4F)][CF_3SO_3] (11)

Yellow greenish; recrystallised from CH_2Cl_2–Et_2O; 50% yield; m.p. 186–188 °C; molar conductivity = 88.2 Ω^{-1} cm^2 mol^{-1}. IR (KBr, cm^{-1}): ν(CN) 2240. ^{1}H-NMR (Me_2CO-d_6): 4.60 (s, 5H, η^5-C_5H_5); 7.39 (t, 2H, H_3, H_5); 7.33–7.79 (q, 2H + Ph, H_2, H_6). $^{13}C\{^1H\}$-NMR ($CDCl_3$): 83.73 (C_5H_5); 106.96 (C1); 117.26 (C3, C5, $^2J(CF) = 23.2$ Hz); 130.36 (CN); 135.30 (C2, C6, $^3J(CF) = 9.0$ Hz); 165.60 (C4, $^1J(CF) = -259.4$ Hz). $^{31}P\{^1H\}$-NMR ($CDCl_3$): 36.1 (2d, $J(P_AP_B) = 38.2$ Hz). Anal. Found: C, 55.09; H, 4.39; N, 1.50; S, 3.34. Calc. for $C_{44}H_{41}F_4NO_5P_2RuS \cdot 1/2CH_2Cl_2$: C, 54.68; H, 4.33; N, 1.43; S, 3.28%.

4.2.12. [Ru(η^5-C_5H_5)((+)-DIOP)-((E)-p-NCCH=$CHC_6H_4NO_2$)][CF_3SO_3] (12)

Orange; recrystallised from CH_2Cl_2–Et_2O; 86% yield; m.p. 154–156 °C; molar conductivity = 87.4

$\Omega^{-1}\,cm^2\,mol^{-1}$. IR (KBr, cm^{-1}): ν(CN) 2220, ν(CH=CH) 1595, $\nu(NO_2)$ 1520, 1340. ^{1}H-NMR (Me_2CO-d_6): 4.58 (s, 5H, η^5-C_5H_5); 6.86 (d, 1H, H_8, $^1J_{HH} = 16.5$ Hz); 7.12 (d, 1H, H_7, $^1J_{HH} = 16.5$ Hz); 7.86 (d, 2H, H_2, H_6); 8.29 (d, 2H, H_3, H_5). $^{13}C\{^1H\}$-NMR ($CDCl_3$): 83.81 (C_5H_5); 101.12 (C8); 124.16 (C3, C5); 128.75–134.10 (CN, C2, C6 + Ph); 138.95 (C1); 148.95 (C4); 149.20 (C7). $^{31}P\{^1H\}$-NMR ($CDCl_3$): 36.1 (2d, $J(P_AP_B) = 38.2$ Hz). Anal. Found: C, 56.08; H, 4.55; N, 2.64; S, 2.92. Calc. for $C_{46}H_{43}F_3N_2O_7P_2RuS$: C, 55.93; H, 4.39; N, 2.83; S, 3.24%.

4.2.13. [Ru(η^5-C_5H_5)((+)-DIOP)-(p-$C_6H_4C_6H_4NO_2$)][CF_3SO_3] (13)

Yellow greenish; recrystallised from CH_2Cl_2–Et_2O; 51% yield; m.p. 297–301 °C; molar conductivity = 79.7 $\Omega^{-1}\,cm^2\,mol^{-1}$. IR (KBr, cm^{-1}): ν(CN) 2220, $\nu(NO_2)$ 1515, 1340. ^{1}H-NMR (Me_2CO-d_6): 4.64 (s, 5H, η^5-C_5H_5); 7.62 (d, 2H, H_2, H_{12}); 8.05 (2d, 4H, H_3, H_{11}, H_6, H_{10}); 8.37 (d, 2H, H_7, H_9). $^{13}C\{^1H\}$-NMR ($CDCl_3$): 82.97 (C_5H_5); 110.88 (C1); 124.28 (C7, C9); 128.34 (C3, C11, C6, C10); 130.49 (CN); 133.30 (C2, C12); 143.86 (C4); 144.93 (C5); 147.89 (C8). $^{31}P\{^1H\}$-NMR ($CDCl_3$): 36.1 (2d, $J(P_AP_B) = 38.2$ Hz). Anal. Found: C, 57.18; H, 4.35; N, 2.59; S, 2.65. Calc. for $C_{50}H_{45}F_3N_2O_7P_2RuS$: C, 57.86; H, 4.37; N, 2.70; S, 3.09%.

4.3. Preparation of [Ru(η^5-C_5H_5)(DPPE)-(p-$NCC_6H_4NO_2$)][$C_4H_4O_7Sb$] (14)

The same procedure as described previously in Section 4.2: [Ru(η^5-C_5H_5)(dppe)Cl] (300 mg, 0.50 mmol); $NCC_6H_4NO_2$ (81 mg, 0.55 mmol); $C_4H_4KO_7Sb$ (812 mg, 2.5 mmol); ruby red, hygroscopic and sensitive to moisture; recrystallised from CH_2Cl_2–Et_2O; 23% yield; m.p. 152–156 °C; molar conductivity = 80.0 $\Omega^{-1}\,cm^2\,mol^{-1}$. IR (KBr, cm^{-1}): ν(CN) 2220, $\nu(NO_2)$ 1520, 1340. ^{1}H-NMR (Me_2CO-d_6): 2.84 (m, 2H, CH_2, DPPE); 2.88 (m, 2H, CH_2, DPPE); 5.12 (s, 5H, η^5-C_5H_5); 7.26 (d, 2H, H_2, H_6); 7.54 (m, 4H, C_6H_5, DPPE); 7.56 (m, 6H, C_6H_5, DPPE); 7.58 (m, 6H, C_6H_5, DPPE); 8.07 (m, 4H, C_6H_5, DPPE); 8.16 (d, 2H, H_3, H_5). $^{13}C\{^1H\}$-NMR ($CDCl_3$): 28.26 (t, CH_2, $^1J_{CP} = 22.90$ Hz, DPPE); 82.86 (C_5H_5); 116.68 (C1); 123.71 (C3, C5); 124.24 (CN); 130.50 (C-*meta*, DPPE); 130.88 (C-*para*, DPPE); 133.18 (C-*ortho*, $^2J_{CP} = 23.76$ Hz, DPPE); 133.78 (C2, C6); 136.65 (C-*ipso*, $J_{CP} = 23.16$ Hz, DPPE); 149.34 (C4). $^{31}P\{^1H\}$-NMR ($CDCl_3$): 79.7 (s). Anal. Found: C, 56.33; H, 4.81; N, 3.21. Calc. for $C_{42}H_{37}N_2O_9P_2RuSb{\cdot}C_2H_5OC_2H_5$: C, 56.20; H, 4.55; N, 2.61%.

4.4. X-ray structures of [Ru(η^5-C_5H_5)((+)-DIOP)-(p-N≡$CC_6H_4NO_2$)][PF_6], [Ru(η^5-C_5H_5)((+)-DIOP)-(p-N≡$CC_6H_4NO_2$)][CF_3SO_3]·$C_2H_5OC_2H_5$ and [Ru(η^5-C_5H_5)((+)-DIOP)(p-N≡CCH_3)][PF_6]

Single crystal diffraction experiments were carried out at r.t. on an Enraf–Nonius MACH3 diffractometer with graphite monchromatised Mo–K_α using the $\omega/2\theta$ scan technique. The unit cell dimensions and orientation matrix were obtained by least-squares refinement of 25 centred reflections. Using the MOLEN software [19], data were corrected for Lorentz and polarisation effects and using Ψ-scans for absorption. The structures were solved by direct methods using SHELXS-97 [20] and refined by full-matrix least squares against F^2 of all data, using SHELXL-97 [21], both programs included in OSCAIL Version 8 [22]. Details for data collection and structure determination are included in Table 5.

All nonhydrogen atoms were refined anisotropically except for the solvent molecule in [RuCp(DIOP)(p-$NCC_6H_4NO_2$)][CF_3SO_3]·$C_2H_5OC_2H_5$ (**16**). All hydrogen atoms were inserted in calculated positions and refined isotropically with a thermal parameter equal to 1.2 times those of the atoms to which they are bonded. In the structure of the acetonitrile complex (**10**) two half molecules of PF_6 were found to be in a twofold screw axis (one in the special position (x, 0, 0) and the other in (0, y, 0.25). The illustrations of the molecular diagrams of the three complexes were drawn with the program ORTEP-II [23] included in the OSCAIL Version 8 [22]. The packing diagram drawings were made with SCHAKAL [24]. The atomic scattering factors and anomalous scattering terms were taken from the International Tables of X-ray Crystallography [25].

4.5. Kurtz powder SHG measurements

The efficiency of SHG is measured using the Kurtz powder method [10]. Our experimental set-up is presented in Fig. 7. The powder sample S is located in a proper sample holder where it is hit by a high-power pulsed laser beam. The sample is on the focus of the parabolic mirror R witch collimates the rear lobule of the SHG light. The collimated beam is focused by the lens L on the photomultiplier PM. The sample holder has a line filter F of adequate wavelength for SHG in order to cut any leak from the fundamental beam or residual florescence from the laser. Neutral density filters N, in the sample holder, allow control of the intensity of SHG light hitting the PM. The PM signal is measured with a 2 GS s^{-1} digital oscilloscope DO which automatically integrates the signal. This integral is proportional to the SHG efficiency and a quantitative value is extracted by comparing it with its corre-

Table 5
Crystal data and structure refinement for [RuCp((+)-DIOP)($NCPhNO_2$)][PF_6] (**15**), [RuCp((+)-DIOP)($NCPhNO_2$)][CF_3SO_3]·$C_2H_5COC_2H_5$ (**16**) and [RuCp((+)-DIOP)($NCCH_3$)][PF_6] (**10**)

Complex	**15**	**16**	**10**
Empirical formula	$C_{43}H_{41}F_6N_2O_4P_3Ru$	$C_{48}H_{41}F_3N_2O_8P_2RuS$	$C_{38}H_{40}F_6NO_2P_3Ru$
Formula weight	957.76	1025.90	850.69
Temperature (K)	293(2)	293(2)	293(2)
Wavelength (Å)	0.71069	0.71069	0.71069
Crystal system	Triclinic	Monoclinic	Orthorhombic
Space group	$P1$	$P2_1$	$C222_1$
Unit cell dimensions			
a	9.900(3)	11.968(2)	15.757(2)
b	10.611(2)	16.559(2)	20.182(2)
c	10.923(2)	13.207(2)	24.364(2)
α	80.047(17)		
β	72.612(18)	113.100(10)	
γ	82.92(2)		
V (Å^3)	1075.4(4)	2407.5(6)	7747.9(14)
Z	1	2	8
D_{calc} (Mg m^{-3})	1.479	1.415	1.459
Absorption coefficient (mm^{-1})	0.546	0.500	0.591
$F(000)$	488	1048	3472
Theta range for data collection (°)	1.95–26.97	1.68–27.97	1.64–24.98
Index ranges	$-12\leq h\leq 12$, $0\leq k\leq 13$, $-13\leq l\leq 13$	$0\leq 0\leq 15$, $0\leq k\leq 21$, $-17\leq l\leq 16$	$-18\leq h\leq 14$, $-14\leq k\leq 23$, $-28\leq l\leq 0$
Reflections collected	4938	6266	7297
Independent reflections	4938 [$R_{int}=0.0000$]	5995 [$R_{int}=0.0341$]	6803 [$R_{int}=0.1394$]
Reflections observed ($>2s$)	3428	4984	4316
Refinement method	Full-matrix least-squares on F^2		
Data/restraints/parameters	4938/3/532	5995/0/560	6803/0/463
Final R indices [$I>2\sigma(I)$]	$R_1=0.0714$	$R_1=0.0475$	$R_1=0.0927$
R indices (all data)	$R_1=0.1121$	$R_1=0.0645$	$R_1=0.1532$
Absolute structure parameter	−0.03(8)	0.00(4)	−0.06(11)
Goodness-of-fit on F^2	1.134	1.067	1.115
Largest difference peak and hole (e Å^{-3})	0.577 and −0.512	0.769 and −0.450	0.991 and −1.302

sponding value from a reference material (urea or KDP) obtained under the same experimental conditions.

The measurements can be performed at two different fundamental wavelengths: 1064 and 1907 nm. The 1064 nm laser pulses are produced directly by the Nd:YAG laser at low power (50 mJ per pulse), this laser produces 40 ns pulses with a repetition rate of 10 Hz. A Raman cell filled with hydrogen produces the 1907 nm laser pulses when pumped by the Nd:YAG laser at high power (1 J per pulse). The duration and repetition rate of this laser pulses are the same as that of the Nd:YAG laser and the energy is about 10 mJ per pulse.

The procedure for the measurements is as follows: samples, grain sizes were not standardised. For this reason signals between individual measurements were seen to vary in some cases by as much as ±20%. The material to be measured was mulled to a fine powder and compacted in a mount and than installed in the sample holder. For a proper comparison with the reference material the measurements should be averaged over several laser thermal cycles. If the sample is not resistant to laser damage then the repetition rate of the shots should be decreased from the normal 10 Hz. The voltage from the PM is measured by the oscilloscope, which is triggered by the signal itself. The photomultiplier voltage and the neutral density filter area were optimised to obtain a good signal to noise relation and prevent the saturation of the photomultiplier. The oscilloscope measures the time integral of the PM voltage automatically, which is proportional to the SHG efficiency. The oscilloscope also performs the average over several laser shots automatically. The reference sample SHG efficiency measurement is performed under the same experimental conditions as that of the test sample.

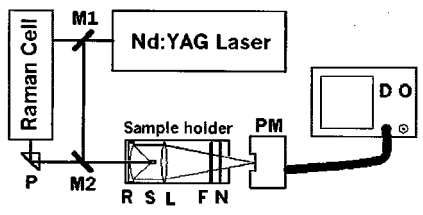

Fig. 7. Experimental set-up for SHG measurements by Kurtz powder technique.

5. Supplementary material

Crystallographic data for the structural analysis have been deposited with the Cambridge Crystallographic Data Centre, CCDC nos. 157900–157902 for compounds **15**, **16** and **10**, respectively. Copies of this information may be obtained free of charge from The Director, CCDC, 12 Union Road, Cambridge CB2 1EZ, UK (Fax: +44-1223-336033; e-mail: deposit@ccdc.cam.ac.uk or www: http://www.ccdc.cam.ac.uk).

Acknowledgements

M. Helena Garcia is very grateful to Professor M.L.H. Green, FRS, University of Oxford, for providing full technical details for the manufacture of the sample holder and also for all the information that made possible the installation of the set-up for Kurtz powder measurements at the University of Lisbon. Junta Nacional de Investigação Científica supported the PhD grant of João Rodrigues (BD/1721/91-IC). This work was partially funded by PRAXIS XXI n° PCEX/C/QUI/96.

References

[1] D.J. Williams, Angew. Chem. Int. Ed. Engl. 23 (1984) 690.
[2] E. Goovaerts, W.E. Wenseleers, M.H. Garcia, G.H. Cross, in: H.S. Nalwa (Ed.), Handbook of Advanced Electronic and Photonic Materials, vol. 9, Academic Press, San Diego, 2001, p. 127, chap. 3.
[3] I.R. Whittall, A.M. McDonagh, M.G. Humphrey, M. Samoc, Adv. Organomet. Chem. 42 (1998) 291.
[4] M.L.H. Green, S.R. Marder, M.E. Thompson, J.A. Bandy, D. Bloor, P.V. Kolisnsky, R.J. Jones, Nature 330 (1987) 360.
[5] A.R. Dias, M.H. Garcia, M.P. Robalo, M.L.H. Green, K.K. Lai, A.J. Pulham, S.M. Klueber, G. Balavoine, J. Organomet. Chem. 453 (1993) 241.
[6] A.R. Dias, M.H. Garcia, J.C. Rodrigues, M.L.H. Green, K.K. Lai, S.M. Klueber, J. Organomet. Chem. 475 (1994) 241.
[7] W. Wenseleers, A.W. Gerbrandij, E. Goovaerts, M.H. Garcia, M.P. Robalo, P.J. Mendes, J.C. Rodrigues, A.R. Dias, J. Mater. Chem. 8 (1998) 925.
[8] W.J. Geary, Coord. Chem. Rev. 7 (1977) 81.
[9] M.H. Garcia, M.P. Robalo, A. Galvão, M.F.M. Piedade, A.R. Dias, E. Goovaerts, W. Wenseleers, J. Organomet. Chem. 619 (2001) 252.
[10] S.K. Kurtz, T.T. Perry, J. Appl. Phys. 39 (1968) 3798.
[11] F.H. Allen, O. Kennard, R. Taylor, Acc. Chem. Res. 16 (1983) 146.
[12] T.J. Johnson, M.R. Bond, R.D. Willett, Acta Crystallogr. Sect. C 44 (1988) 1890.
[13] J. Zyss, J.L. Oudar, Phys. Rev. A 26 (1982) 2016.
[14] J. Zyss, J.L. Oudar, Phys. Rev. A 26 (1982) 2028.
[15] J. Zyss, J.F. Nicoud, M. Coquillay, J. Chem. Phys. 81 (1984) 4160.
[16] J. Zyss, D.S. Chemla, Quadratic nonlinear optics and optimization of the second-order nonlinear optical response of molecular crystals, in: D.S. Chemla, J. Zyss (Eds.), Nonlinear Optical Properties of Organic Molecules and Crystals, vol. I, Academic Press, New York, 1987, p. 118 (chap. II).
[17] D.D. Perrin, W.L.F. Amarego, D.R. Perrin, Purification of Laboratory Chemicals, 2nd ed., Pergamon, New York, 1980.
[18] G.S. Ashby, M.I. Bruce, I.B. Tomkins, R.C. Walli, Aust. J. Chem. 32 (1979) 1003.
[19] C.K. Fair, MOLEN, An Interactive Intelligent System for Crystal Structure Analysis, Enraf–Nonius, Delft, The Netherlands, 1994.
[20] G.M. Sheldrick, Acta Crystallogr. Sect. A 46 (1990) 67.
[21] G.M. Sheldrick, SHELXL-97, A Program for Refining Crystal Structures, University of Göttingen, Göttingen, Germany, 1997.
[22] C.K. Johnson, M.N. Burnett, ORTEPIII, Report ORNL-6895, Oak Ridge National Laboratory, Tennessee, USA, 1996.
[23] P. McArdle, J. Appl. Crystallogr. 28 (1995) 65.
[24] E. Keller, SCHAKAL-97, Graphical Representation of Molecular Models, University of Freiburg, Germany, 1997.
[25] International Tables for X-ray Crystallography, vol. IV, Kynoch Press, Birmingham, UK, 1974.
[26] J.F. Costello, S.G. Davies, R.M. Highcock, M.E.C. Polywka, M.W. Poulter, T. Richardson, G.G. Roberts, J. Chem. Soc. Dalton Trans. (1997) 105.
[27] O.Y. Carreon, M.A. Leyva, J.M. Fernandez-G, A. Penicaud, Acta Crystallogr. Sect. C 53 (1997) 301.